

Supplemental Information for Single-atom photocatalysis in 2D fullerene structure for water splitting and CO₂ reduction

Miao Cheng,[†] Kang Li,[‡] Naixu Li,^{*,†} and Jie Guan^{*,‡}

*[†]School of Physics, School of Chemistry and Chemical Engineering, Southeast University,
Nanjing 211189 PRC*

*[‡]Key Laboratory of Quantum Materials and Devices of Ministry of Education, School of
Physics, Southeast University, Nanjing 211189 PRC*

E-mail: naixuli@seu.edu.cn; guanjie@seu.edu.cn

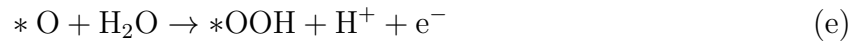
Gibbs Free Energy calculations

For hydrogen evolution reaction (HER), oxygen evolution reaction (OER) and CO₂ reduction reaction (CO₂RR) pathways in acidic environments, the reaction steps can be written as follows.^{1,2}

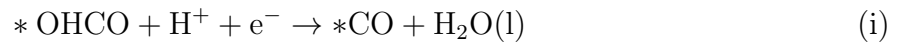
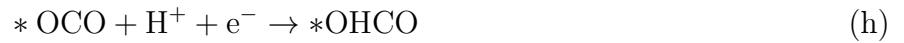
HER:



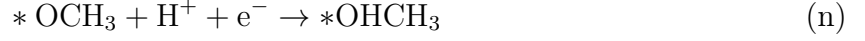
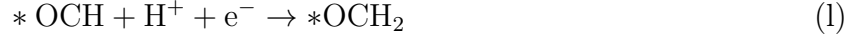
OER:



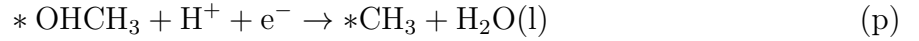
CO₂RR to CO:



If not desorbed, the *CO can be further reduced to generate CH₃OH:



If not desorbed, the *OHCH₃ can be further reduced to generate CH₄:



The computational hydrogen electrode (CHE) model was used to calculate the free energy for the reaction step involving proton-electron couple ($\text{H}^+ + \text{e}^-$), where the free energy of ($\text{H}^+ + \text{e}^-$) was set equal to that of $1/2\text{H}_2$ at an electrode potential of $U = 0$ relative to the reversible hydrogen electrode.³ In the absence of an applied potential, the corresponding free energy differences for all the reaction steps are given as follows.

HER:

$$\Delta G_a = G_{*H} - G_* - \frac{1}{2}G_{H_2} \quad (\text{S1})$$

$$\Delta G_b = G_* + G_{H_2} - G_{*H} - \frac{1}{2}G_{H_2} = G_* + \frac{1}{2}G_{H_2} - G_{*H} \quad (\text{S2})$$

OER:

$$\Delta G_c = G_{*OH} + \frac{1}{2}G_{H_2} - G_* - G_{H_2O} \quad (S3)$$

$$\Delta G_d = G_{*O} + \frac{1}{2}G_{H_2} - G_{*OH} \quad (S4)$$

$$\Delta G_e = G_{*OOH} + \frac{1}{2}G_{H_2} - G_{*O} - G_{H_2O} \quad (S5)$$

$$\Delta G_f = G_* + \frac{1}{2}G_{H_2} + G_{O_2} - G_{*OOH} \quad (S6)$$

CO₂RR:

$$\Delta G_g = G_{*OCO} - G_* - G_{CO_2} \quad (S7)$$

$$\Delta G_h = G_{*OHCO} - G_{*OCO} - \frac{1}{2}G_{H_2} \quad (S8)$$

$$\Delta G_i = G_{*CO} + G_{H_2O} - G_{*OHCO} - \frac{1}{2}G_{H_2} \quad (S9)$$

$$\Delta G_j = G_{CO} + G_* - G_{*CO} \quad (S10)$$

$$\Delta G_k = G_{*OCH} - G_{*CO} - \frac{1}{2}G_{H_2} \quad (S11)$$

$$\Delta G_l = G_{*OCH_2} - G_{*OCH} - \frac{1}{2}G_{H_2} \quad (S12)$$

$$\Delta G_m = G_{*OCH_3} - G_{*OCH_2} - \frac{1}{2}G_{H_2} \quad (S13)$$

$$\Delta G_n = G_{*OHCH_3} - G_{*OCH_3} - \frac{1}{2}G_{H_2} \quad (S14)$$

$$\Delta G_o = G_* + G_{CH_3OH} - G_{*OHCH_3} \quad (S15)$$

$$\Delta G_p = G_{*CH_3} + G_{H_2O} - G_{*OHCH_3} - \frac{1}{2}G_{H_2} \quad (S16)$$

$$\Delta G_q = G_{*CH_4} - G_{*CH_3} - \frac{1}{2}G_{H_2} \quad (S17)$$

$$\Delta G_r = G_{CH_4} + G_* - G_{*CH_4} \quad (S18)$$

Supplemental Figures and Tables

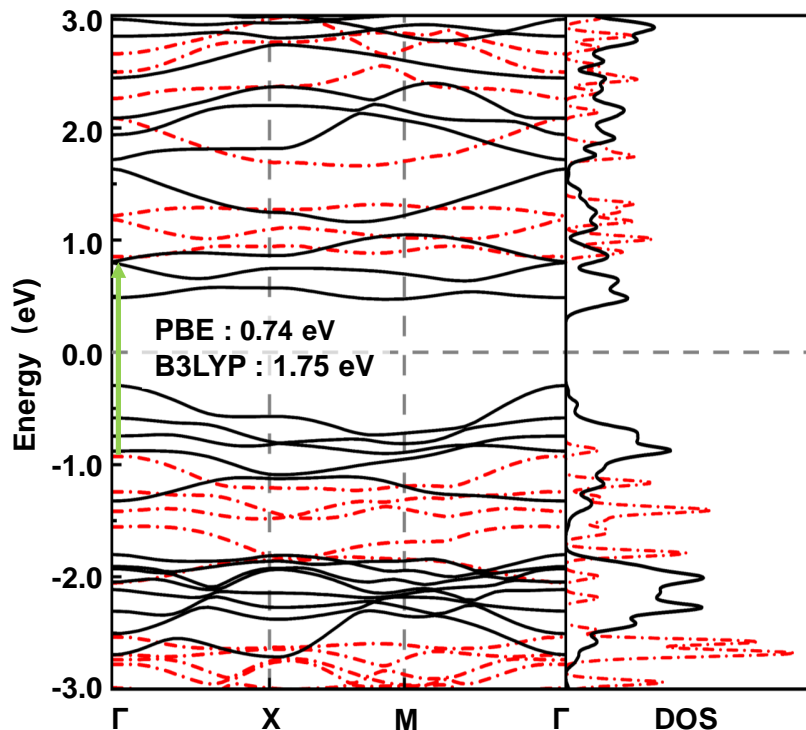


Figure S1: Electronic band structure and the density of states (DOS) for qHP-C₆₀. The results based on PBE and B3LYP functionals are shown by the black solid and red dashed lines, respectively. The direct band gap are shown by the green arrow. Both PBE and B3LYP values of the band gap are given.

Table S1: The free energy barriers of HER at $pH = 0$ for all the M@C₆₀ (M = metal) structures and the corresponding best reaction sites as labeled in Figure S4.

metal	ΔG_{*H}	site	metal	ΔG_{*H}	site
Li	-0.035	C4	Ca	0.054	C4
Na	-0.044	C4	Sr	-0.054	C6
K	-0.032	C6	Ba	0.045	C4
Rb	-0.045	C6	Sc	0.074	C4
Cs	-0.010	C6	Y	-0.035	C6
Tl	0.012	C4			

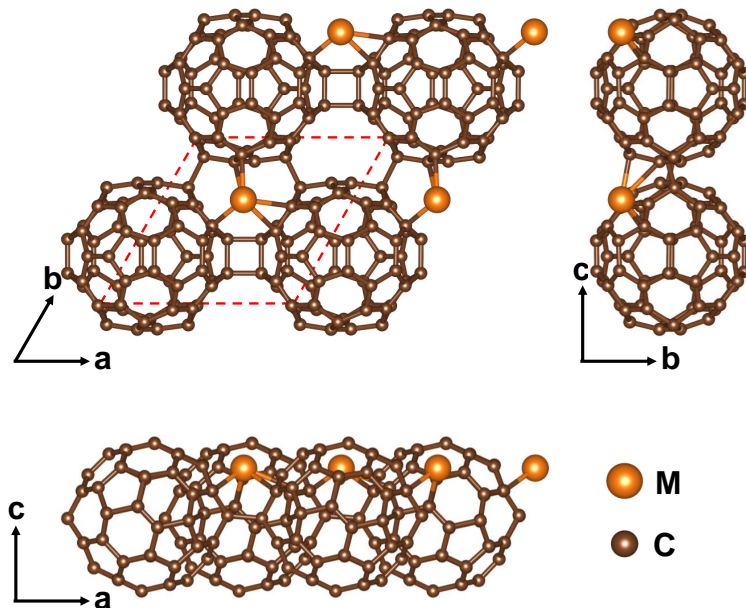


Figure S2: Equilibrium structure of $M@C_{60}$.

Table S2: The free energy barriers of the rate-determining step (RDS) in OER at $pH = 0$ for all the $M@C_{60}$ ($M = \text{metal}$) structures, as well as the corresponding reaction step and best reaction site.

Metal	ΔG_{RDS}	RDS	site
Li	1.79	*OH \rightarrow *O	C4
Na	1.76	*OH \rightarrow *O	C2
K	1.85	*O \rightarrow *OOH	C3
Rb	1.80	*O \rightarrow *OOH	C3
Cs	1.82	*O \rightarrow *OOH	C3
Ca	1.72	*O \rightarrow *OOH	C2
Sr	1.66	*OH \rightarrow *O	C3
Ba	1.69	*O \rightarrow *OOH	C3
Sc	1.71	*O \rightarrow *OOH	C4
Y	1.73	*O \rightarrow *OOH	C2
Tl	1.69	*O \rightarrow *OOH	C6

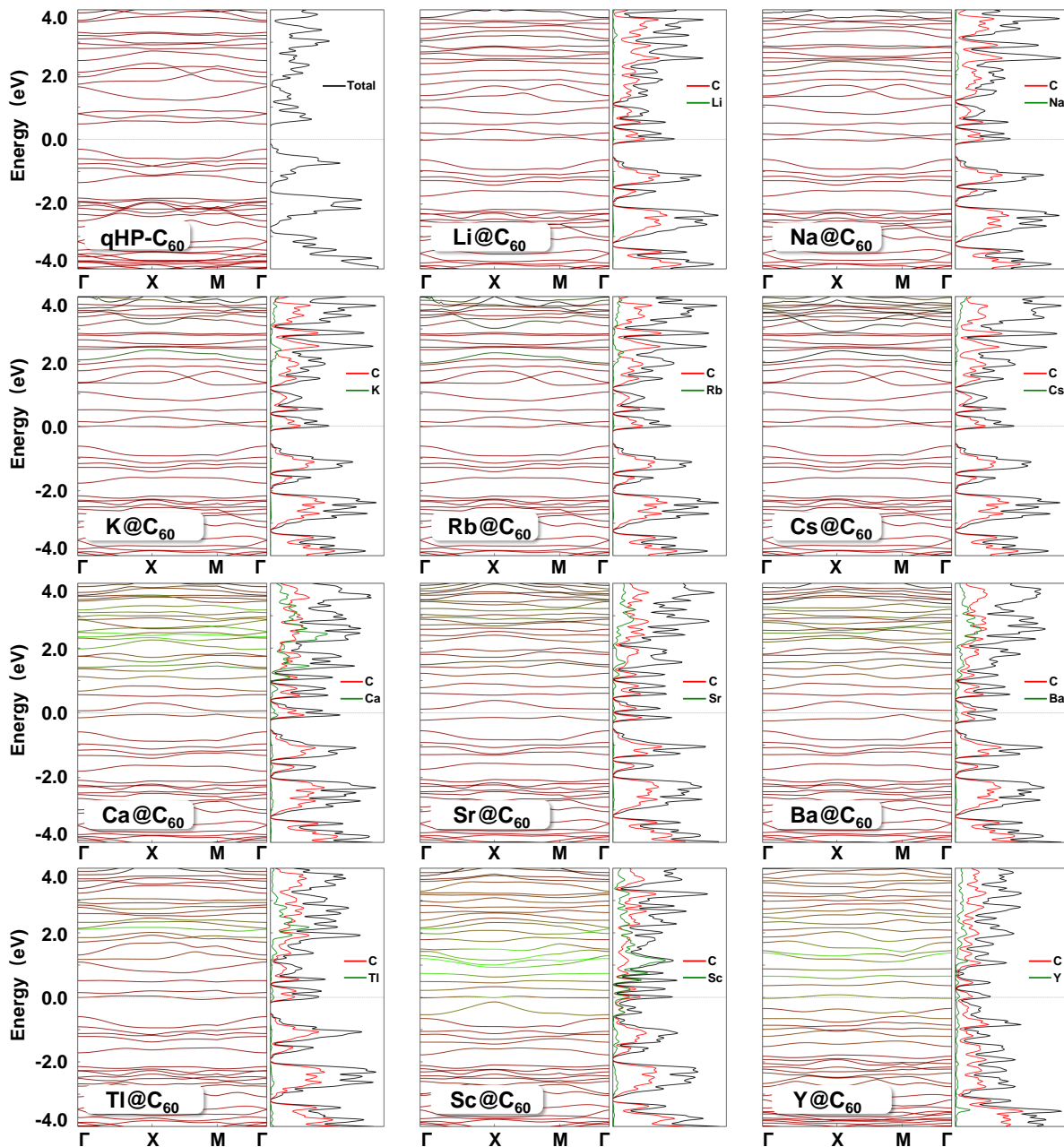


Figure S3: Projected electronic band structure and density of states (DOS) for pristine qHP-C₆₀ and M@C₆₀ with different metals.

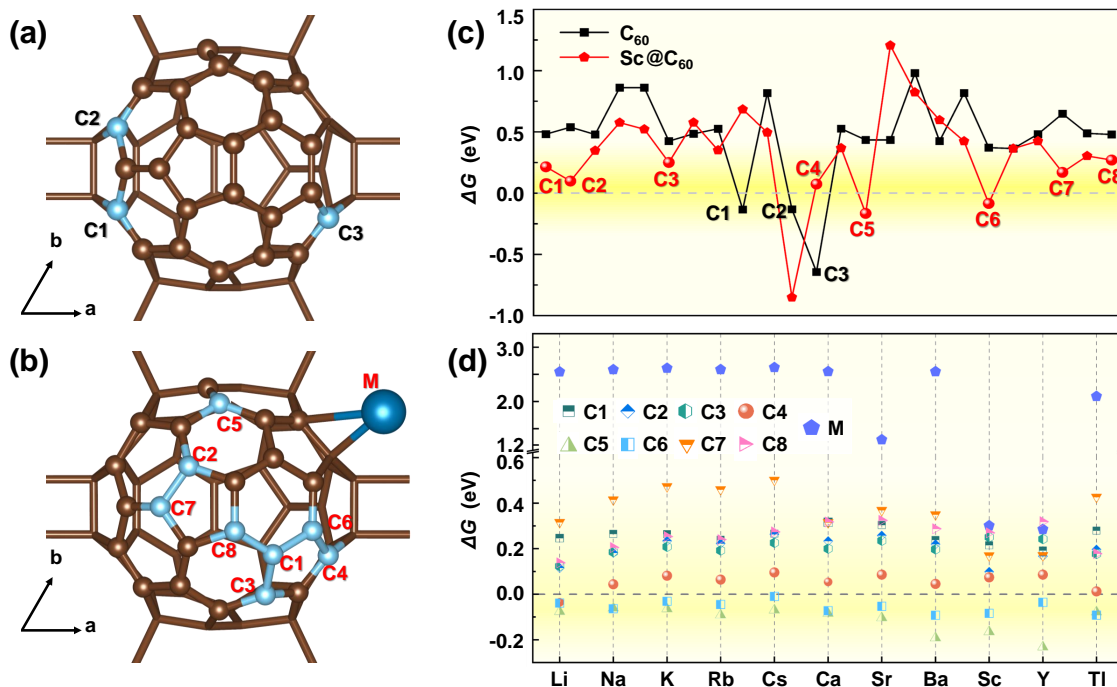


Figure S4: The comparison of different reaction sites for attaching H atom on both pristine qHP-C₆₀ and M@C₆₀. All the possible C sites on the surface, as the atoms indicated by the ball model in (a) pristine qHP-C₆₀ and (b) M@C₆₀, are considered. The free-energy changes (ΔG) of forming the ^{*}H intermediate at different C sites under $pH = 0$ in pristine qHP-C₆₀ (black color) and Sc@C₆₀ (red color), which is selected as the representative of the doped metals, are presented in (c). For pristine qHP-C₆₀, the sites adjacent to the sp³-hybridized C (C1-C3), as highlighted by the cyan color in (a), exhibit much lower ΔG than the other sites. The sites with the lowest ΔG in absolute value are the equivalent C1 and C2. For Sc@C₆₀, we choose the sites with the ΔG absolute value smaller than 0.3 eV, as labeled from C1 to C8 and highlighted in (b), and extend them to all the other doped metals. The ΔG of forming ^{*}H for M@C₆₀ with all the investigated metals at the selected eight C sites and the M site are compared in (d). The best sites and the corresponding ΔG are summarized in Table S1.

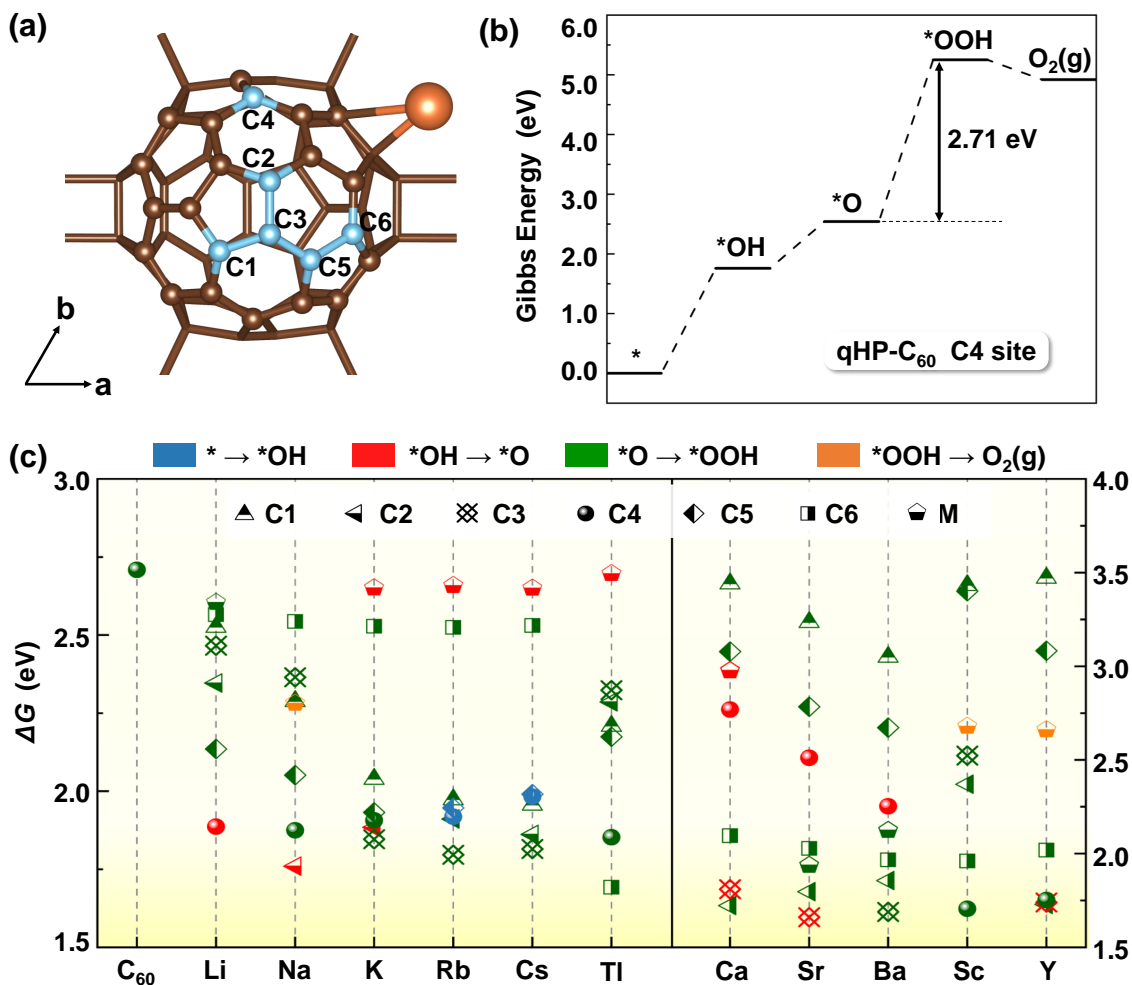


Figure S5: The comparison of different reaction sites for OER in pristine qHP-C₆₀ and M@C₆₀. The possible C sites on the surface close to the M atoms, as the atoms indicated by the ball model in (a), are considered. The free energies of all the intermediates during the OER pathway in pristine qHP-C₆₀ at different C sites were calculated and the free energy diagram under $pH = 0$ for the best reaction site, labeled as C4 in (a), is shown in (b). Since the forming of *OOH is the rate-determining step (RDS) for pristine qHP-C₆₀, the *OOH intermediate at different sites for Sr@C₆₀, which is selected as the representative of the doped metals, was calculated. It is found that the -OOH radical can only be stably adsorbed at the C1-C6 sites, as highlighted by the cyan color in (a). We thus take these six C sites and the M site for consideration and extend them to all the other doped metals. The ΔG of the RDS during the OER pathway for all the investigated metals at different sites are presented in (c). The data for different reaction sites and the corresponding different RDSs are distinguished by shape and color, respectively. The best sites and the corresponding ΔG are summarized in Table S2.

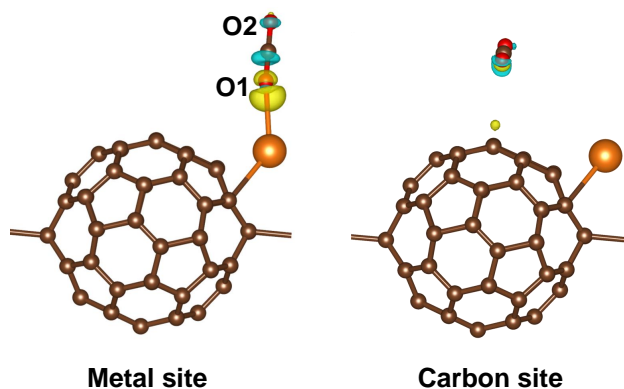


Figure S6: Differential change density distribution for adsorbing CO_2 on the M and C sites of Sr@C_{60} . The isosurfaces are 0.003 and 0.0006 e/Bohr^3 for the M and C sites, respectively. A significantly stronger interaction between CO_2 and the substrate at the M site than the C site is observed.

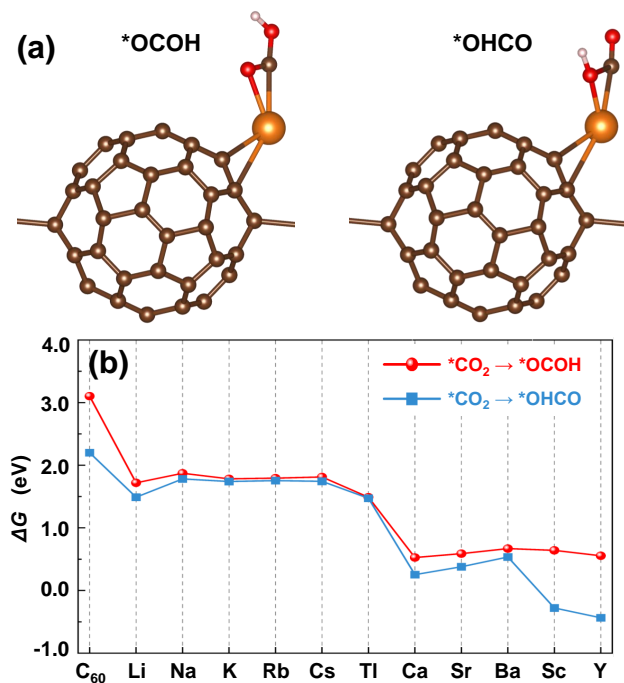


Figure S7: (a) Structures of the hydrogenation on different O atoms in the adsorbed CO_2 and (b) the corresponding free energy change (ΔG) for pristine qHP- C_{60} and M@C_{60} with different metals.

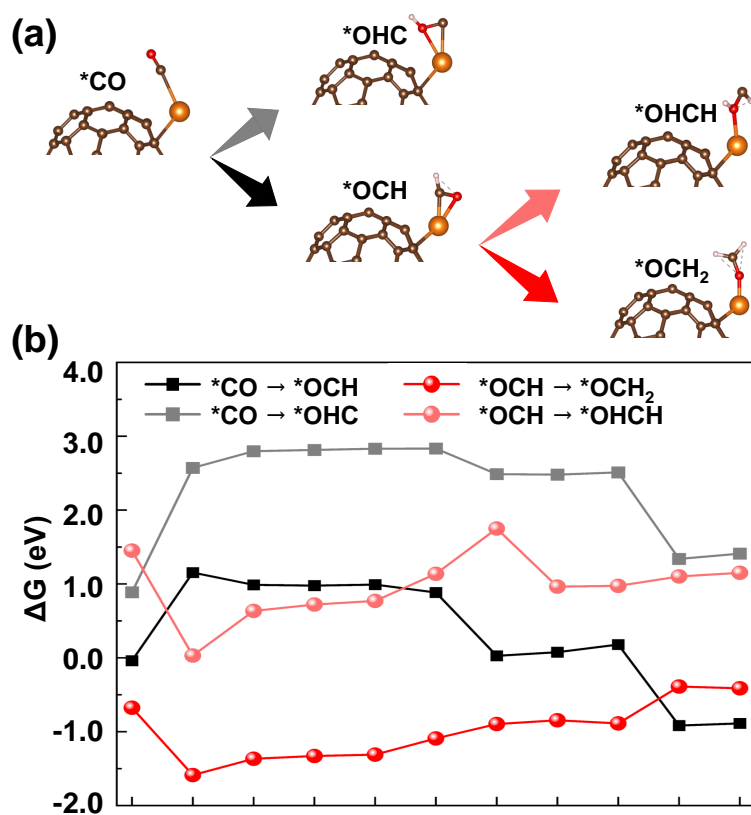


Figure S8: (a) The hydrogenation of the *CO intermediate at different sites during the CO₂RR pathway and the corresponding free energy change (ΔG) at $pH = 0$ for M@C₆₀ with different metals.

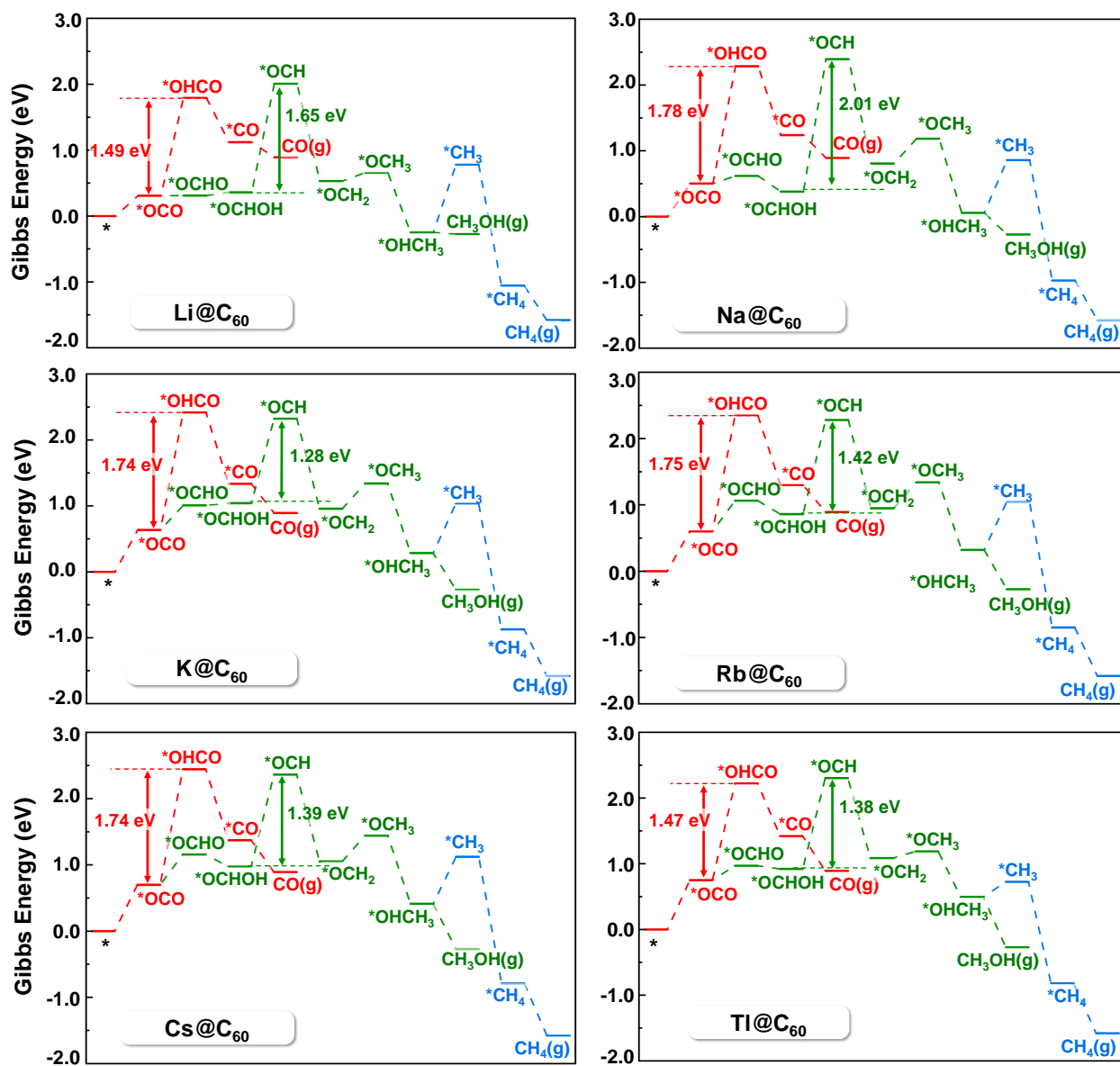


Figure S9: Free energy diagrams of CO₂RR at $pH = 0$ for M@C₆₀ with M = Li, Na, K, Rb, Cs, and Tl.

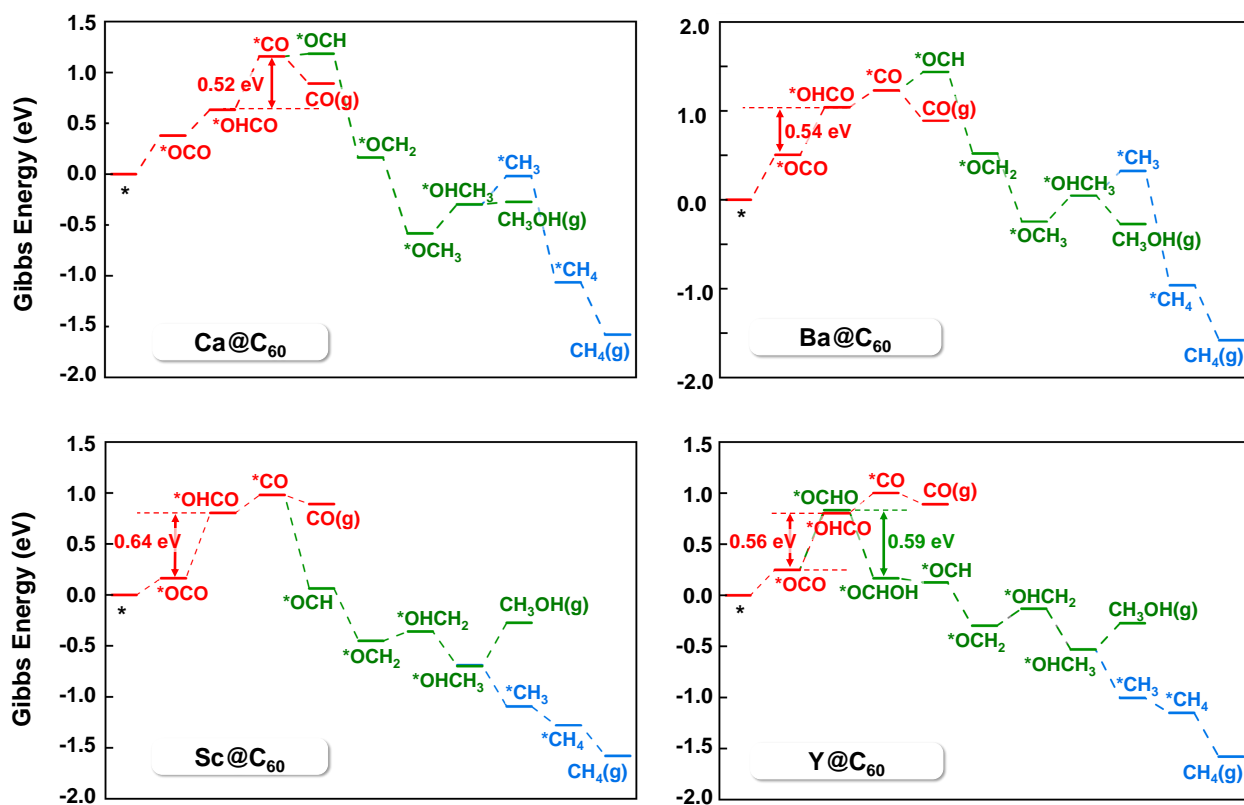


Figure S10: Free energy diagrams of CO₂RR at $pH = 0$ for M@C₆₀ with M = Ca, Ba, Sc, and Y.

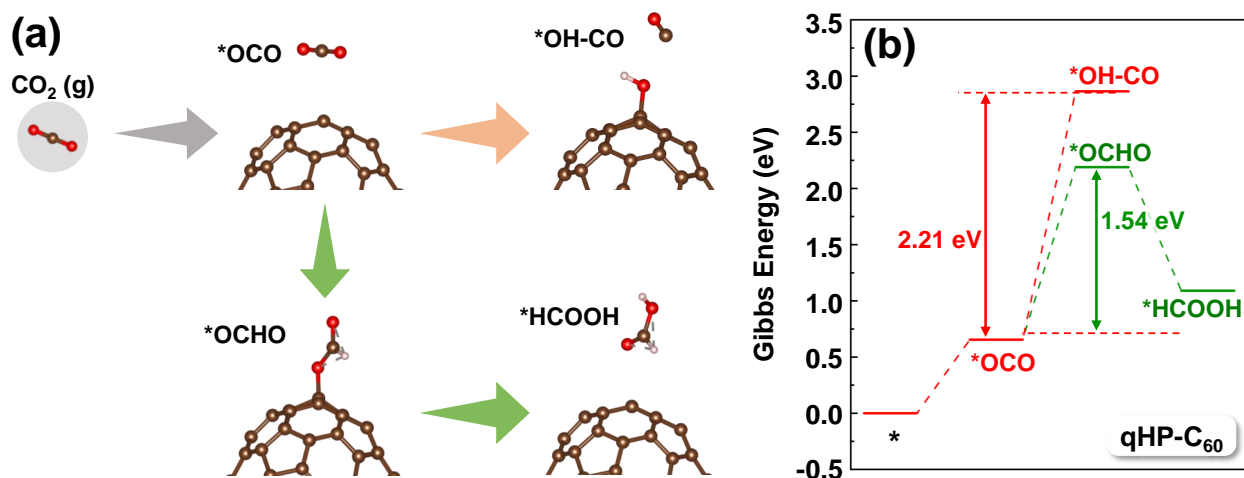


Figure S11: (a) Reaction pathway of CO₂RR for pristine qHP-C₆₀ and (b) the corresponding free energy diagram.

References

- (1) Ali, S.; Ismail, P. M.; Humayun, M.; Bououdina, M.; Qiao, L. Tailoring 2D Metal-Organic Frameworks for Enhanced CO₂ Reduction Efficiency through Modulating Conjugated Ligands. *Fuel Process. Technol.* **2024**, *255*, 108049.
- (2) Yasin, G.; Ali, S.; Ibraheem, S.; Kumar, A.; Tabish, M.; Mushtaq, M. A.; Ajmal, S.; Arif, M.; Khan, M. A.; Saad, A.; Qiao, L.; Zhao, W. Simultaneously Engineering the Synergistic-Effects and Coordination-Environment of Dual-Single-Atomic Iron/Cobalt-sites as a Bifunctional Oxygen Electrocatalyst for Rechargeable Zinc-Air Batteries. *ACS Catal.* **2023**, *13*, 2313–2325.
- (3) Nørskov, J. K.; Rossmeisl, J.; Logadottir, A.; Lindqvist, L.; Kitchin, J. R.; Bligaard, T.; Jónsson, H. Origin of the Overpotential for Oxygen Reduction at a Fuel-Cell Cathode. *J. Phys. Chem. B*, **2004**, *108*, 17886–17892.